JOURNAL OF SPACECRAFT AND ROCKETS
Vol. 36, No. 3, May–June 1999

Mars Polar Lander Aerothermodynamic and Entry Dispersion Analysis

Eric M. Queen,* F. McNeil Cheatwood,* Richard W. Powell,* and Robert D. Braun*
NASA Langley Research Center, Hampton, Virginia 23681
and
C. Thomas Edquist†
Lockheed Martin Astronautics, Denver, Colorado 80127

An analysis of the aerothermodynamics and trajectory dispersions experienced by the Mars Polar Lander entry system was performed and is documented herein. Because the Mars Polar Lander aeroshell (forebody) is based on the Mars Pathfinder aeroshell, the Pathfinder aerodynamic database was used by Lockheed Martin Astronautics for their trajectory analyses. However, the afterbodies of the two vehicles are different. The effects of the different geometry and different trajectory were isolated, and the Pathfinder aerodynamic database was found to be appropriate for the Mars Polar Lander entry work with minor modifications. Independent heating calculations were conducted, which agree with the heating analyses done at Lockheed Martin Astronautics. Also, it was determined that, at the expected parachute-deploy conditions, the area of recirculated flow extends less than two body lengths behind the vehicle. The extent of this recirculation region can impact successful parachute deployment. A six-degree-of-freedom simulation of the entry phase was developed, including much of the actual flight code for the attitude control autopilot. This simulation was exercised to evaluate the autopilot and overall system performance during entry and to evaluate response to dispersions that might affect the entry trajectory. It was determined that the autopilot keeps the vehicle oriented correctly for the disturbances modeled. Also, the six-degree-of-freedom simulation was used in a Monte Carlo analysis to determine the expected footprint and altitude at parachute deploy.

Nomenclature

C_A = axial force coefficient, nondimensionalized by $\frac{1}{2}\rho_\infty V_\infty^2 S$
C_m = moment coefficient, nondimensionalized by $\frac{1}{2}\rho_\infty V_\infty^2 SL$
C_N = normal force coefficient, nondimensionalized by $\frac{1}{2}\rho_\infty V_\infty^2 S$
$CF\iota$ = MarsGRAM density climate factor at ι km altitude, where ι is 0, 1, 5, 15, 30, 50, 75 km
h = altitude, km
Kn = Knudsen number
L = reference length, m
M = Mach number
p = pressure, N/m^2
q = surface heating, W/cm^2
S = reference area, m^2
T_w = wall temperature, K
V = velocity, m/s
x = radial distance from body axis (in symmetry plane), m
z = axial distance from nose, m
α = angle of attack, deg
γ = flight-path angle, deg
ρ = atmospheric density, kg/m^3
σ = standard deviation
τ = atmospheric opacity in MarsGRAM climate factor model

Introduction

THE Mars Polar Lander will be the first scientific mission to the polar regions of Mars. On arriving at Mars, the lander vehicle will make a direct entry into the Martian atmosphere and decelerate to a landing near the south pole. An aeroshell similar to that used by Mars Pathfinder will be used to protect the lander during its passage through the atmosphere. When the vehicle has decelerated to about Mach 2, a parachute will open to further slow the vehicle. The vehicle will ride the parachute until it is close enough to the ground to make a soft landing using controlled rocket thrust.

The lander vehicle was designed and built by Lockheed Martin Astronautics (LMA), which has done extensive work designing and evaluating the vehicle through all of the phases of its mission. In this analysis, several specific aspects of the entry phase are examined. Despite the high degree of commonality between the Mars Pathfinder and Mars Polar Lander aeroshells, the differences warranted evaluation of the use of the Pathfinder database for Mars Polar Lander. Also, a six-degree-of-freedom (DOF) dynamical analysis of the entry trajectory was desired, especially with respect to uncertainties in aerodynamics, atmospheric conditions, vehicle properties, etc.

The Mars Polar Lander aeroshell (forebody) is essentially a scaled duplicate of the Pathfinder aeroshell. However, the afterbodies of the two vehicles have some subtle, but potentially significant, differences. Inasmuch as the Mars Pathfinder data have been used for the Mars Polar Lander, this study attempts to quantify the following: 1) the effects on aerodynamics of differences between Mars Polar Lander and Pathfinder geometry and trajectory, 2) the heating environment of the Mars Polar Lander, and 3) the extent of the afterbody recirculation region at parachute deploy.

A six-DOF simulation of the entry phase was developed, including much of the actual flight code for the attitude control autopilot. This simulation was exercised to evaluate the autopilot and overall system performance during entry. In addition, a sensitivity analysis was performed to determine the systems response to variations in variables that might affect the entry trajectory. The six-DOF simulation was used in a Monte Carlo analysis to determine the expected footprint and altitude at parachute deploy.

Aerothermodynamic Analysis

The aerothermodynamics portion of the NASA Langley Research Center (LaRC) effort consists of three tasks: 1) evaluate the use of the Mars Pathfinder aerodynamic database for the Mars Polar Lander atmospheric entry and modify that database as required, 2) calculate the heating rate at the estimated peak heating condition

Received Nov. 15, 1998; revision received Jan. 20, 1999; accepted for publication Feb. 22, 1999.

*Research Engineer, Vehicle Analysis Branch. Member AIAA.
†Senior Staff Engineer, Aerophysics Flight Systems. Member AIAA.

along the aeroshell, and 3) provide insight into the flight environment at parachute deploy.

The Mars Pathfinder database was developed by NASA LaRC in support of the Pathfinder project.[1] That database is in the form of a Fortran subroutine, which is called by a trajectory code. A number of modifications have been made to the original subroutine since it was delivered to LMA. Thus, as a first step in this analysis, a comparison was made between LMA's database and LaRC's database for Mars Pathfinder. The good agreement shown in Fig. 1 indicates that the databases were comparable, though not identical.

The remainder of the aerothermodynamics analysis employed computational fluid dynamics (CFD) calculations. The code LAURA[2–4] was used to solve the thin-layer Navier–Stokes equations. An eight-species, two-temperature gas model for Mars was used, along with a radiative equilibrium wall temperature boundary condition. A supercatalytic material was specified, yielding a recombination of the gas to freestream composition at the vehicle surface. Because the Mars Polar Lander has an active control system that should keep the vehicle near zero angle of attack, an evaluation of axial force at various trajectory points via axisymmetric solutions serves as the foundation of this investigation.

A volume grid is required to define the domain over which the governing equations are solved. LMA provided a vehicle geometry definition about which a volume grid was built. Because the forebodies of Mars Pathfinder and Mars Polar Lander are very similar, the grid generation effort focused on the shoulder region and afterbody (Fig. 2). A grid with 70 cells in the axial direction and 32 cells in the body-normal direction was employed for these axisymmetric solutions. The integrated aerodynamic coefficients C_A, C_N, and C_m provide the measure for solution convergence. The solution for a given grid is said to be converged when 1000 iterations yields a change of less than 0.1% for each of these quantities. Adaptions to the grid are discontinued when the converged aerodynamic coefficients for successive grids display a change of less than 0.1%.

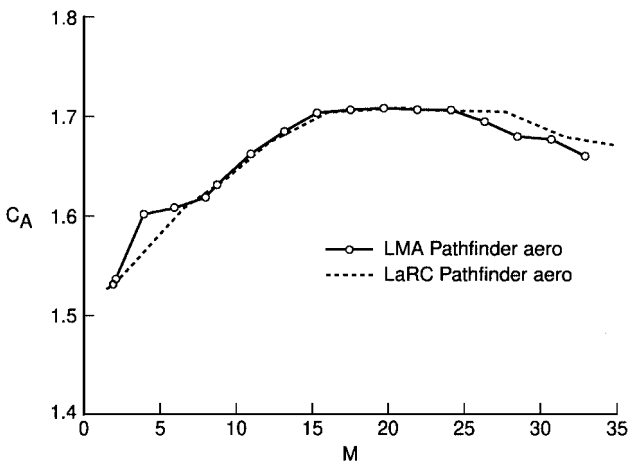

Fig. 1 Comparison of Mars Pathfinder aerodynamics subroutines.

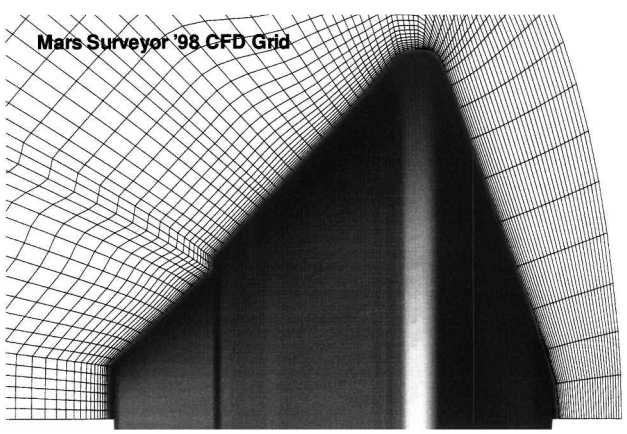

Fig. 2 Grid resolution for CFD calculations.

Table 1 Results from CFD solutions over Mars Polar Lander geometry along Mars Pathfinder trajectory

M	V, m/s	Mars Polar Lander	Mars Pathfinder	Difference
1.9	420	1.597	1.529	0.068
31.6	6592	1.681	1.679	0.002

Table 2 Freestream conditions for solutions over Mars Polar Lander geometry

h, km	M	V, m/s	ρ, kg/m^3	T, K
33.7	30.81	6091	2.342^{-4}	156.43
15.8	6.141	1213	2.655^{-3}	156.20
14.1	4.687	925.7	3.406^{-3}	156.10
12.1	3.534	697.8	4.473^{-3}	156.09
9.74	2.551	503.8	6.281^{-3}	156.12

Table 3 Axial force results from solutions over Mars Polar Lander geometry along Mars Polar Lander trajectory

			Pathfinder C_A		Scale factor	
M	V, m/s	C_A	fcn(M)[a]	fcn(V)	fcn(M)	fcn(V)
30.81	6091	1.705	1.684	1.692	1.012	1.008
6.141	1213	1.593	1.609	1.612	0.990	0.988
4.687	925.7	1.580	1.610	1.632	0.981	0.968
3.534	697.8	1.575	1.591	1.616	0.990	0.975
2.551	503.8	1.577	1.555	1.550	1.014	1.017

[a]fcn, Function.

Variations between Mars Pathfinder and Mars Polar Lander aerodynamics can be traced to two sources: differences in geometry and in trajectory. In an attempt to isolate the geometry contribution, axisymmetric solutions at the Mars Pathfinder peak heating and parachute-deploy conditions were calculated over the Mars Polar Lander geometry. The calculated axial force coefficients are given in Table 1 along with values supplied by the Mars Pathfinder aerodatabase subroutine. There is very little effect of geometry differences on the aerodynamics at high-Mach-number condition (because afterbody effects are negligible). This should be the case until the freestream Mach number drops below Mach 10. However, the afterbody gains influence at low Mach numbers, as is evident at parachute deploy where a difference in C_A of approximately 4% is seen. Using freestream conditions from the Mars Polar Lander nominal trajectory, five axisymmetric solutions were calculated about the Mars Polar Lander geometry. The conditions for these solutions are provided in Table 2. The axial force coefficients for these solutions are presented in Table 3 along with values supplied by the Mars Pathfinder subroutine. Note that the trajectory differences impact even the high Mach number result.

The axial forces from these seven LAURA solutions are plotted in Figs. 3 and 4, as functions of Mach number and velocity, respectively. Because the Mars Pathfinder subroutine provides aerodynamics as a function of Mach number or velocity, results are plotted vs both. Figures 3 and 4 also include the CFD values that anchor the Mars Pathfinder database. These results are converted to scale factors (a ratio of Mars Polar Lander to Pathfinder values) as functions of Mach number and velocity, respectively, also shown in Table 3. These scale factors should be applied to the Pathfinder aerodynamic database in subsequent Mars Polar Lander analysis and design efforts.

For the heating analysis, both an axisymmetric and a three-dimensional solution were calculated at the predicted peak heating flight conditions. The three-dimensional solution, which does not include the afterbody, is at 5-deg angle of attack. The grid has 24 cells in the axial direction, 18 cells in the circumferential direction, and 64 cells in the body-normal direction. Figure 5 shows flooded color contours of the surface heating (based on a radiative equilibrium wall temperature) for the three-dimensional case.

Figure 6 shows the symmetry plane heating distributions for both the axisymmetric and three-dimensional solutions. Figure 7 shows the corresponding radiative equilibrium wall temperature

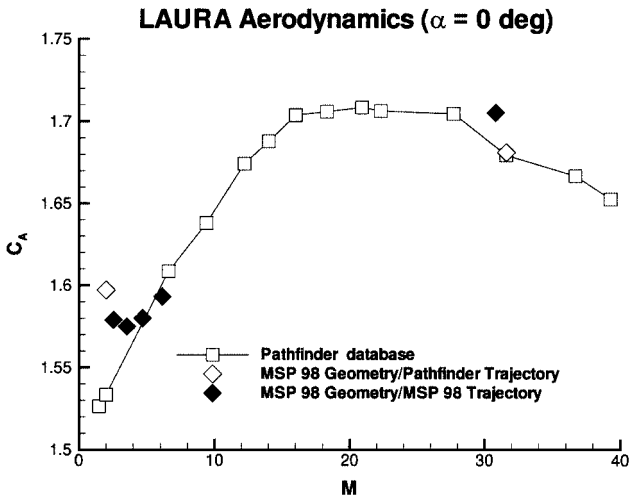

Fig. 3 Comparison of Mars Pathfinder and Mars Polar Lander axial forces (as a function of Mach number).

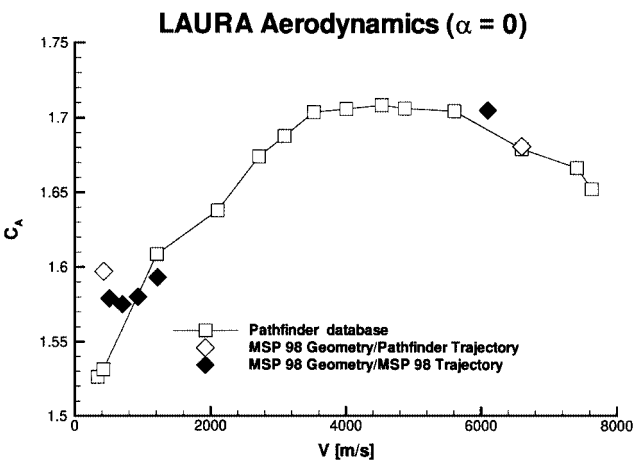

Fig. 4 Comparison of Mars Pathfinder and Mars Polar Lander axial forces (as a function of velocity).

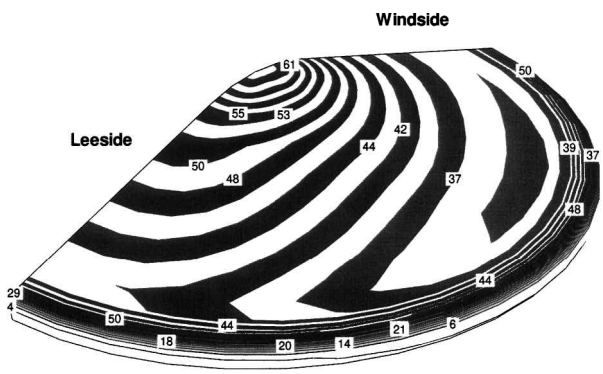

Fig. 5 Surface heating contours at peak heating: $\alpha = 5$ deg.

distributions for the two solutions. The three-dimensional solution does not adequately resolve the stagnation region in the axial direction. It also does not have a node at the stagnation point. As a result, the heating in that region is not accurately predicted. The aerodynamic coefficients from this solution are compared with Mars Pathfinder values in Table 4.

The axisymmetric grid has 88 cells axially and 64 cells normal to the body. As a result, it has twice as many cells as the three-dimensional grid in the stagnation region (and it has a node at the stagnation point). Because the stagnation point of both solutions is on the spherical cap, the axisymmetric heating result in that region should agree with the three-dimensional values. Figure 8 shows three heat pulses for the re-entry (corresponding to nominal, overshoot, and undershoot trajectories) determined using the Sutton and

Table 4 Aerodynamic coefficients at peak heating ($t = 100$ s) for $\alpha = 5$ deg

Coefficient	Mars Polar Lander	Mars Pathfinder	Difference
C_A	1.628	1.661	−0.033
C_N	0.01327	0.01312	0.00015
C_m^a	−0.00539	−0.00561	0.00022

[a] About the Mars Pathfinder reference point, 0.662 m aft of nose.

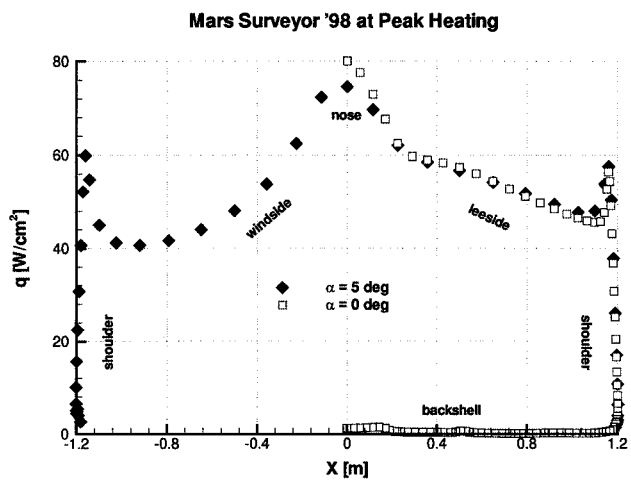

Fig. 6 Symmetry plane surface heating distribution at peak heating.

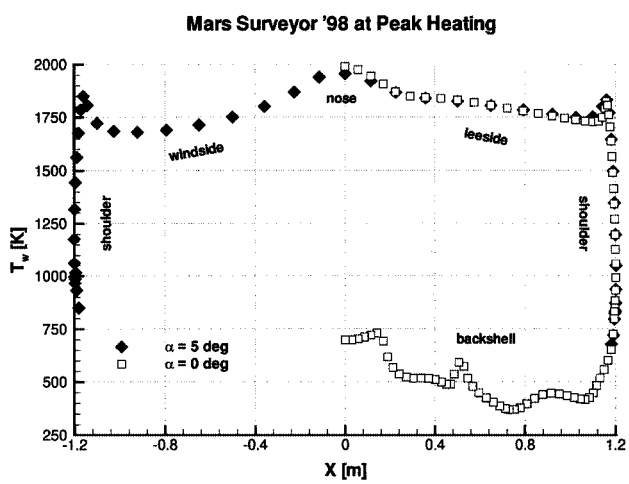

Fig. 7 Symmetry plane wall temperature distribution at peak heating.

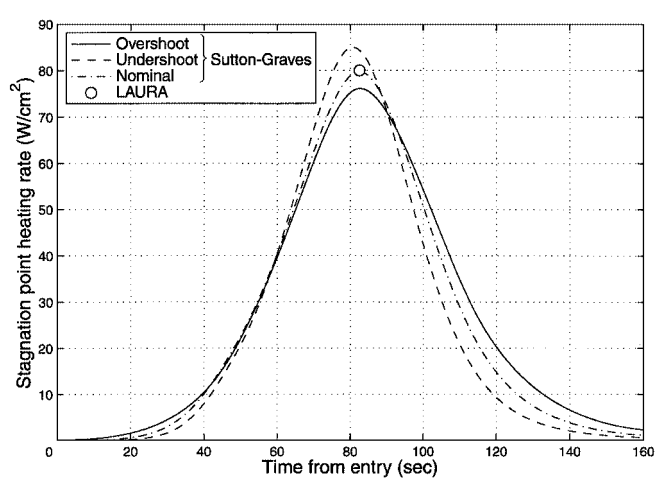

Fig. 8 LAURA CFD peak heating solution shown with heat pulse from engineering method.

Graves[5] engineering method. As shown in Fig. 8, this stagnation value of approximately 80 W/cm^2 agrees well with the LMA estimate of 79.95 W/cm^2 for the nominal trajectory. However, from LMA CFD results the value is 69 W/cm^2 (approximately 86% of the LAURA value). These two CFD solutions are based on different wall catalysis conditions: The LAURA solution assumes freestream chemical composition, whereas the LMA solution uses an equilibrium composition. The former produces larger gradients at the wall, so that the LAURA result should be a higher (more conservative) number. For both the axisymmetric and three-dimensional case, the shoulder heating is seen to be approximately 75% of the stagnation value, and so a monolithic heatshield sized to the stagnation conditions should be adequate for the entire forebody of the vehicle. Heating levels fall off rapidly on the backshell, where only a minimal level of thermal protection is required.

The sonic line for the inviscid portion of the shock layer is on the spherical cap for the axisymmetric case. As shown in Fig. 9, that same character exists on the leeside symmetry plane of the three-dimensional solution ($M < 1$ in the gray region). That is, the shock layer is predominately supersonic. On the windside, however, the sonic line shifts to the shoulder of the vehicle, and a large portion of the shock layer is subsonic. A similar result was observed for the Mars Pathfinder aeroshell.[1] As a result, the axisymmetric heating results closely track the leeside symmetry plane values (see Figs. 6 and 7).

Both an axisymmetric and a three-dimensional solution were calculated at the predicted flight conditions for parachute deploy. The three-dimensional solution is at 2-deg angle of attack and includes the flowfield about the afterbody. The grid has 70 cells in the axial direction, 18 cells in the circumferential direction, and 32 cells in the body-normal direction. Figure 10 shows streamlines for the three-dimensional solution. Note that the recirculation region is confined to the first 1.5 body lengths aft of the vehicle, as indicated by the streamline pattern. The extent of this recirculation region can

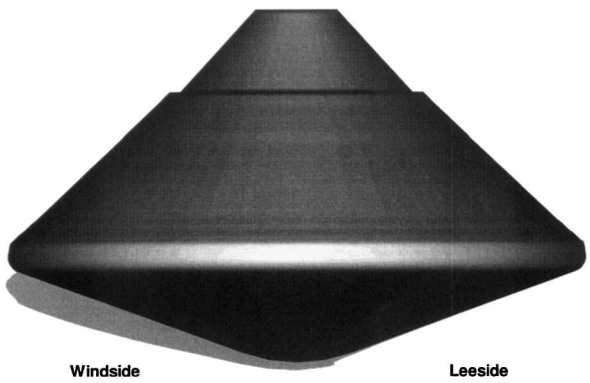

Fig. 9 Sonic line at peak heating: α = 5 deg.

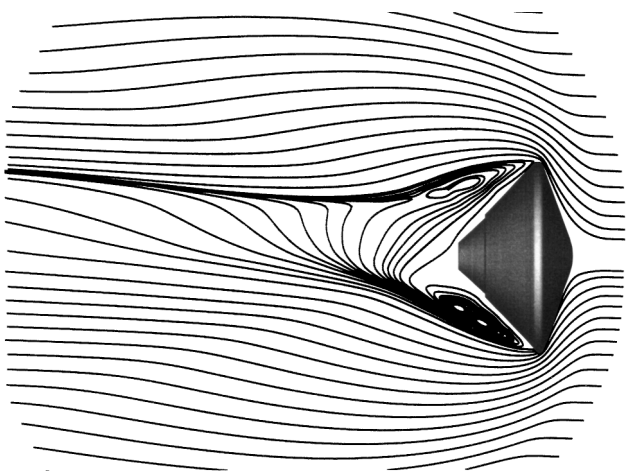

Fig. 10 Streamlines at parachute deploy: α = 2 deg.

Table 5 Aerodynamic coefficients at parachute deploy (t = 213 s) for α = 2 deg

Coefficient	Mars Polar Lander	Mars Pathfinder	Difference
C_A	1.564	1.555	0.009
C_N	−0.000194	0.00671	−0.00690
C_m^a	−0.00441	−0.00343	−0.00098

[a]About the Mars Pathfinder reference point, 0.662 m aft of nose.

impact successful parachute deployment. The aerodynamic coefficients from this solution are compared with Mars Pathfinder values in Table 5.

Trajectory Analysis

The trajectory analysis was based on a six-DOF simulation. This simulation was used to determine sensitivities to a variety of factors that might affect the trajectory. Two Monte Carlo analyses were performed to show the expected parachute-deploy footprint for varying degrees of center-of-gravity (c.g.) dispersions.

The simulation was based on the six-DOF program 6DPOST.[6] 6DPOST is a general purpose trajectory simulation tool that allows detailed modeling of the vehicle rigid-body dynamics. POST formed the basis of the six-DOF simulations for the Mars Pathfinder Project.[1] The atmosphere model used was MarsGRAM 3.7 (Ref. 7). MarsGRAM includes climate factors, which are adjusted to force the MarsGRAM density profile to agree with more detailed global circulation models. The climate factors used in this study were provided by the Jet Propulsion Laboratory (JPL) and were generated as a function of atmospheric opacity τ by the following relations:

$$CF0 = 1.067199 + 0.06050333 \times (\tau - 0.2)$$

$$CF5 = 1.007162 + 0.08974667 \times (\tau - 0.2)$$

$$CF15 = 1.021097 + 0.18632333 \times (\tau - 0.2)$$

$$CF30 = 0.947960 + 0.28399867 \times (\tau - 0.2)$$

$$CF50 = 0.847850 + 0.09117033 \times (\tau - 0.2)$$

$$CF75 = 1.900000 + 3.05294200 \times (\tau - 0.2)$$

where $CF0$ is the density climate factor at altitude of 0 km, $CF5$ is the density climate factor at 5 km, etc. The value of the ground-level pressure climate factor (CFP) was 1.3. Aerodynamics were generated from the Pathfinder database as earlier amended. The vehicle mass properties were provided by LMA. The inertial measurement unit (IMU) model was provided by NASA Johnson Space Center, based on LMA specifications.[8] The autopilot was provided by LMA. This autopilot is essentially the flight code with an additional model to calculate forces and moments due to the thrusters.

Figure 11 shows the angle-of-attack history for the cases of a nominal c.g. position, vertical c.g. offset −2.5 mm, and vertical c.g. offset +2.5 mm. The effect of a negative c.g. offset is to make the vehicle fly at a more positive angle of attack and vice versa. For this vehicle, a positive angle of attack results in a downward lift force. Thus, the negative c.g. offset (positive α) case flies a shorter trajectory because it is lift down. Similarly, the positive c.g. offset flies lift up, resulting in a longer trajectory. The initial time for Fig. 11 occurs at the assumed atmospheric interface, when the vehicle is 3522.2 km from the center of the planet. There are two regions of instability evident, one at approximately 75 s the other at approximately 110 s. These same static instabilities were predicted for Pathfinder and observed in the flight data.[9] For three cases varying vertical c.g. position, the autopilot maintains the angle of attack within 5 deg.

Listed in Table 6 are 39 of the 40 variables that were perturbed in the six-DOF simulation to determine the sensitivity of the trajectory to variations of each variable. The atmospheric density at arrival, which is intended to model the effects of a global level dust storm, was also perturbed by use of the appropriate profile from Fig. 12. The values for initial flight-path angle γ were provided by JPL: the

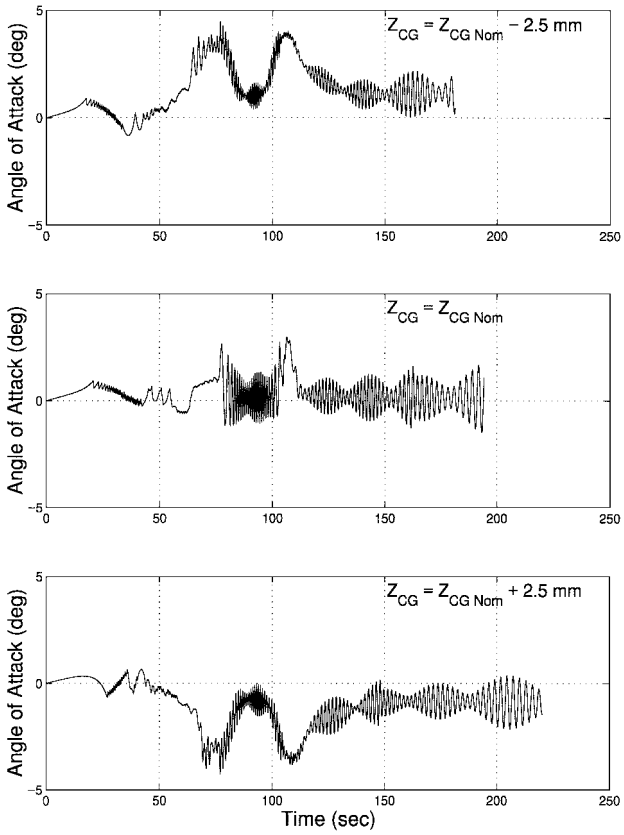

Fig. 11 Angle-of-attack history.

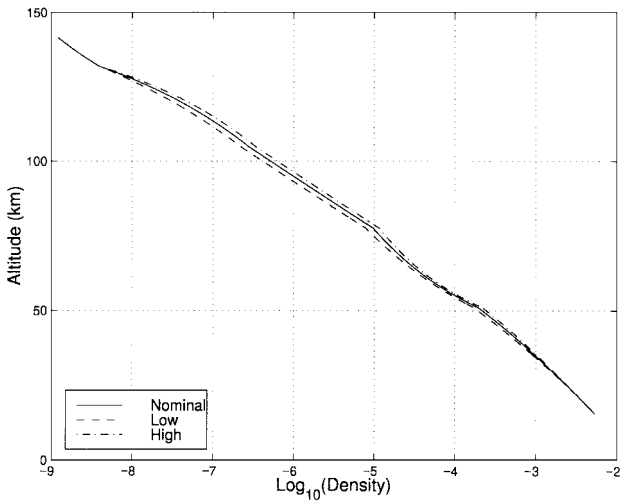

Fig. 12 Logarithm of atmospheric density for three climate factor cases.

variables marked (U) in the "Nominal value" column are drawn from uniform distributions; otherwise variables are drawn from Gaussian distributions with the 3-σ values given in the "Range" column. The variables with range marked "+" are treated as additive perturbations; those marked "×" are multiplicative. The nominal, high, and low atmosphere density profiles are shown in Fig. 12. These density profiles correspond to τ values of 0.35, 0.5, and 0.2, respectively.

The eight variables that had the largest effect on range to nominal deploy site are shown in Fig. 13. (For each variable, the effect of positive and negative perturbations are shown.) The perturbations in the aerodynamic terms were divided into several flight regimes, and variations in each flight regime were considered independently. Variations could be either in free molecular ($Kn > 0.1$), hypersonic ($M > 10$, $Kn < 0.001$), or supersonic ($M < 5$) regions. Between these regions, values were interpolated.

Table 6 Monte Carlo uncertainties

Variable	Nominal value	Range
Lift (rarified)	Table	+(−0.1, 0.1)
Drag (rarified)	Table	×(0.9, 1.1)
Pitch moment (rarified)	Table	+(−0.1, 0.1)
Lift ($M > 10$)	Table	+(−0.05, 0.05)
Drag ($M > 10$)	Table	×(0.975, 1.025)
Drag ($M < 5$)	Table	×(0.9, 1.1)
Pitch moment ($M > 10$)	Table	+(−0.003, 0.003)
Pitch moment ($M < 5$)	Table	+(−0.005, 0.005)
C_{mq} ($M > 10$)	Table	×(0.85, 1.15)
C_{mq} ($M < 5$)	Table	×(0.85, 1.15)
Lift ($M < 5$)	Table	+(−0.08, 0.08)
Spacecraft mass, kg	487.6	+(−2, 2)
Axial c.g. position, mm	0.6149	+(−2.5, 2.5)
Lat c.g. offset dist, mm	0 (U)	+(−2.5, 2.5)
Lat c.g. offset dir, deg	0 (U)	+(0, 360)
Mass inertia I_{xx}, kg-m^2	214.027	×(0.95, 1.05)
Mass inertia I_{yy}, kg-m^2	142.076	×(0.95, 1.05)
Mass inertia I_{zz}, kg-m^2	136.059	×(0.95, 1.05)
Mass inertia I_{xy}, kg-m^2	0.8923	+(−3, 3)
Mass inertia I_{xz}, kg-m^2	−0.4819	+(−3, 3)
Mass inertia I_{yz}, kg-m^2	−10.559	+(−3, 3)
Initial bank angle, deg	0 (U)	+(−0.25, 0.25)
Initial α, deg	0 (U)	+(−0.5, 0.5)
Initial sideslip angle, deg	0 (U)	+(−0.5, 0.5)
Initial pitch rate, deg/s	0 (U)	+(−0.25, 0.25)
Initial yaw rate, deg/s	0 (U)	+(−0.25, 0.25)
Initial roll rate, deg/s	0 (U)	+(−0.25, 0.25)
Roll thruster 1, lb	1	×(0.95, 1.05)
Roll thruster 2, lb	1	×(0.95, 1.05)
Roll thruster 3, lb	1	×(0.95, 1.05)
Roll thruster 4, lb	1	×(0.95, 1.05)
Aft thruster 5, lb	5.2	×(0.95, 1.05)
Aft thruster 6, lb	5.2	×(0.95, 1.05)
Aft thruster 7, lb	5.2	×(0.95, 1.05)
Aft thruster 8, lb	5.2	×(0.95, 1.05)
MarsGRAM param τ	0.35 (U)	+(−0.15, 0.15)
Atmosphere update distance, km	0.5 (U)	+(0, 4.5)
Initial γ, deg	−13.25	−13.76, −12.84

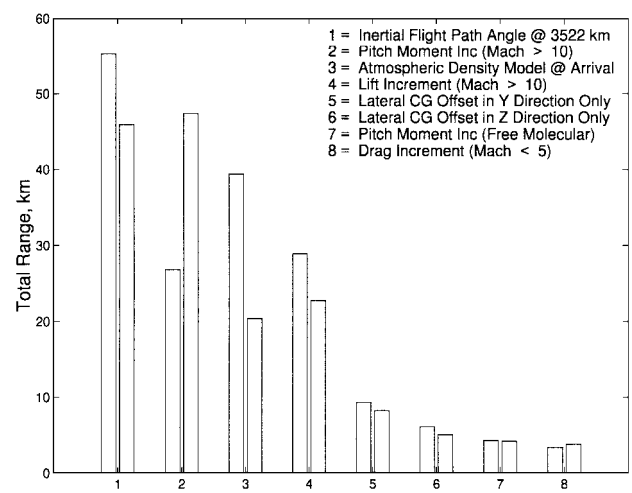

Fig. 13 Largest contributors to range errors.

The variable that has largest impact on total range is initial flight-path angle, followed by pitching moment increment above Mach 10. A variation in pitching moment will cause the vehicle to fly at an off-nominal angle of attack and, thus, to fly either a steeper or shallower trajectory than the nominal. The atmospheric density is the next most influential, followed by c.g. offsets in the Y and Z direction, free-molecular pitching moment, and supersonic drag increment. Figure 14 shows the variables that most influence the reaction control system (RCS) propellant usage during entry. Figure 15 shows the sensitivity of parachute-deploy altitude to

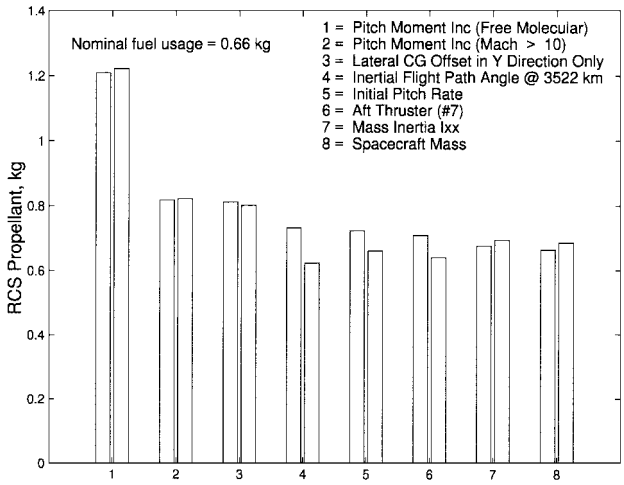

Fig. 14 Largest contributors to RCS usage.

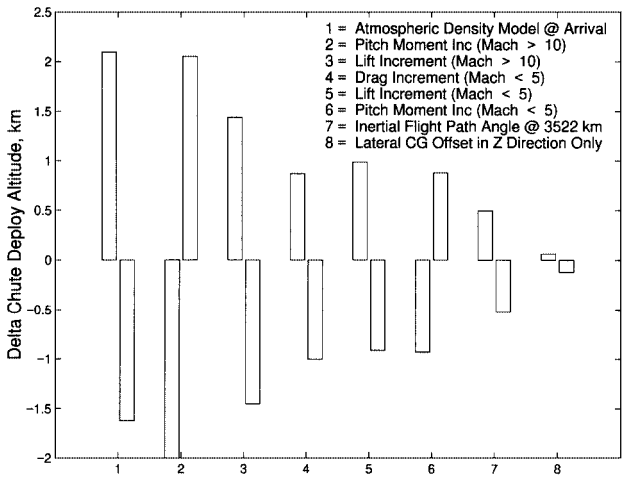

Fig. 15 Largest contributors to parachute-deploy altitude errors.

the most influential variables sorted by absolute value of altitude change.

Following the sensitivity analysis, a Monte Carlo analysis was performed using the same 39 variables as inputs as well as random atmosphere perturbations and navigation errors (see Table 6). Because the atmospheric density model and the climate factors both model density changes in the atmosphere, only the climate factors were used in the Monte Carlo analysis. The IMU was initialized using the nominal state at a radius of 3522.2 km. Figure 16 is a scatter plot of the latitude and longitude of a 2000-case Monte Carlo run. Though the median value is very near the stated target of 75°S, 160°E (Ref. 10), the mean is roughly 74.7°S, 159.3°E, which is approximately 20 km short of the target. Amazingly, the final vehicle mass is slightly less than original estimates.[10] This results in a lower ballistic coefficient, which may account for the short trajectory. Figure 17 shows the range to the nominal parachute-deploysite for the same 2000 cases, 99% of which are within 91.35 km of the target. The RCS fuel usage (shown in Fig. 18) is less than 1.21 kg of for 99% of the cases. The parachute-deploy altitude is shown in Fig. 19. The mean altitude is slightly higher than the nominal,[10] possibly due to the lighter mass already mentioned. In 99% of the cases, there is a difference from the nominal of 3.21 km or less. Note that the mean parachute-deploy altitude is about a kilometer above that predicted by LMA.[10] Figure 20 shows Mach number vs altitude at parachute-deploy. The parachute was deployed at a navigated velocity of 493.8 m/s. Thus, for any given altitude, the only changes in chute deploy Mach number are due to changes in the temperature, which is determined by the climate factors used. There is a great deal of structure apparent in Fig. 20 that was not shown in the LMA results.[10] This discrepancy is probably due to the way the parachute-deploycriterion was modeled within the two simulations.

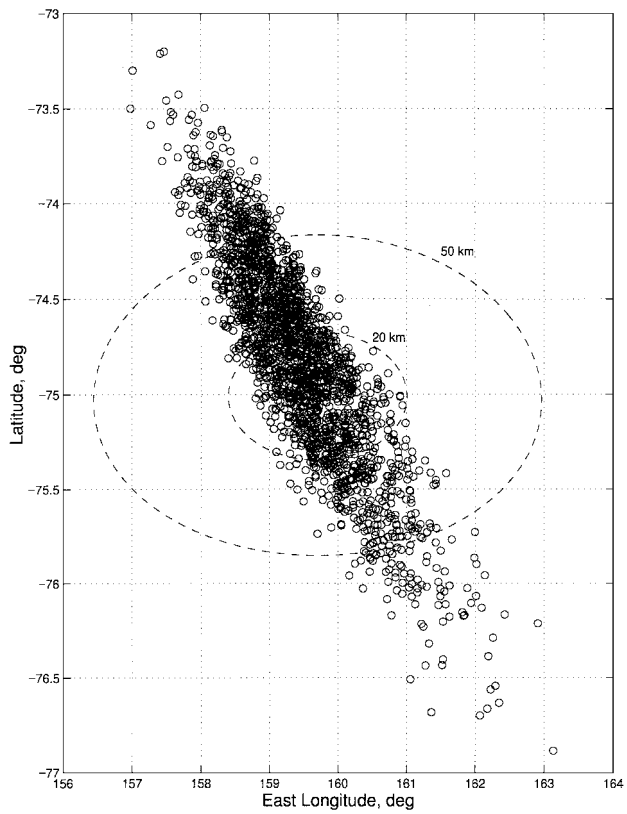

Fig. 16 Location of parachute deploy for 2000 Monte Carlo cases.

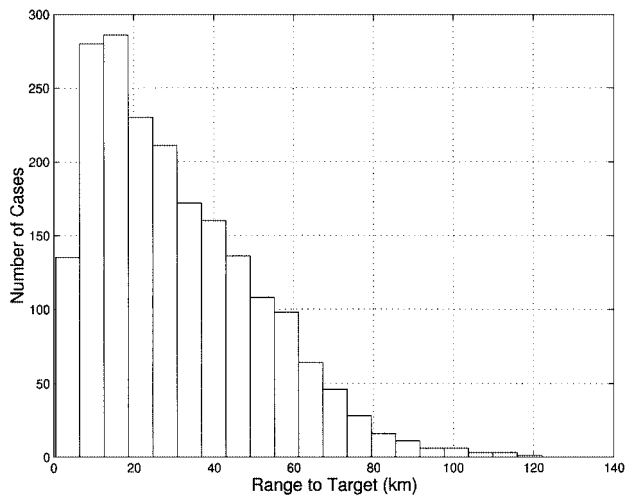

Fig. 17 Distribution of range errors for 2000 Monte Carlo cases.

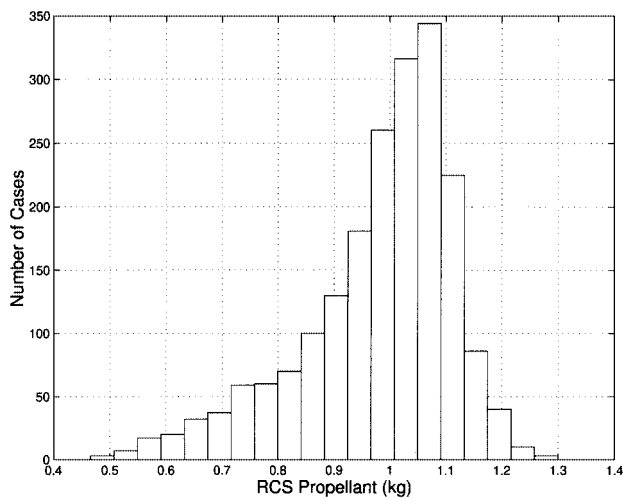

Fig. 18 Distribution of RCS usage for 2000 Monte Carlo cases.

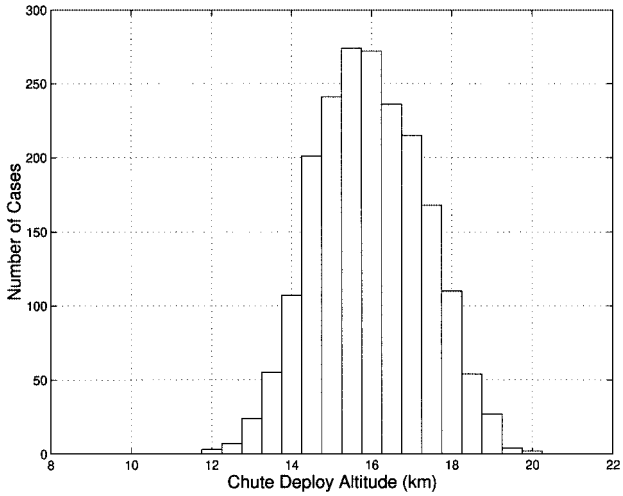

Fig. 19 Distribution of parachute-deploy altitude for 2000 Monte Carlo cases.

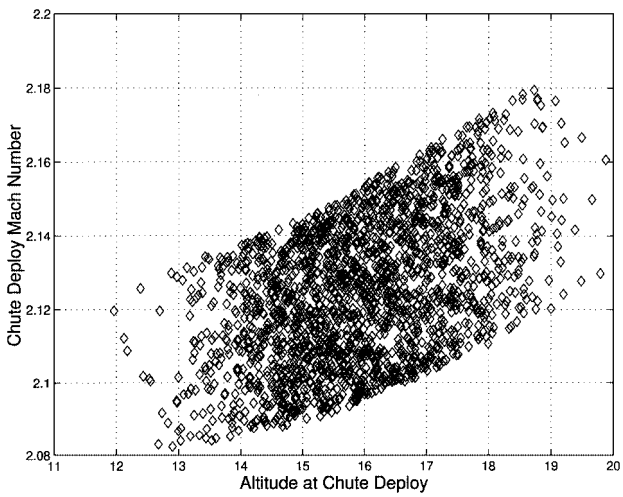

Fig. 20 Relative values of Mach and altitude at parachute deploy for 2000 Monte Carlo cases.

The first Monte Carlo analysis was performed assuming that the vertical c.g. position was within 2.5 mm of the nominal value. To determine the effects of larger c.g. offsets, the Monte Carlo analysis was repeated, with twice the c.g. variation and the off-diagonal moments of inertia. Figure 21 shows that the footprint for the larger dispersions is only slightly larger (99% of cases within 103.4 km of the target point). The RCS propellant usage stays essentially the same (Fig. 22) (99% of cases used less than 1.24-kg propellant), and the change in parachute-deploy altitude is small (Fig. 23) (99% of cases changed parachute-deploy altitude by 3.78 km or less).

Whereas these parachute-deploy footprints were considered acceptable, techniques were sought to reduce the size of the footprints. The largest contributor to range error was the flight-path angle at atmospheric interface, as can be seen from Fig. 13. The variation in flight-path angle is limited by the approach geometry and the capabilities of the Deep Space tracking network. The third largest contributor, atmopheric density on the day of arrival, is impossible to predict with great accuracy. Improvements in the flight-path angle and the atmospheric density were, thus, considered impractical. Contributions from the pitching moment above Mach 10 and the lift coefficient above Mach 10 might be reduced by further wind-tunnel and/or CFD work. Unfortunately, budget constraints precluded significant work in this area. However, inasmuch as the aerodynamic forces and moments are strong functions of vehicle attitude, it might be possible to reduce the parachute-deploy footprint by more tightly constraining the vehicle attitude, in particular the angle of attack.

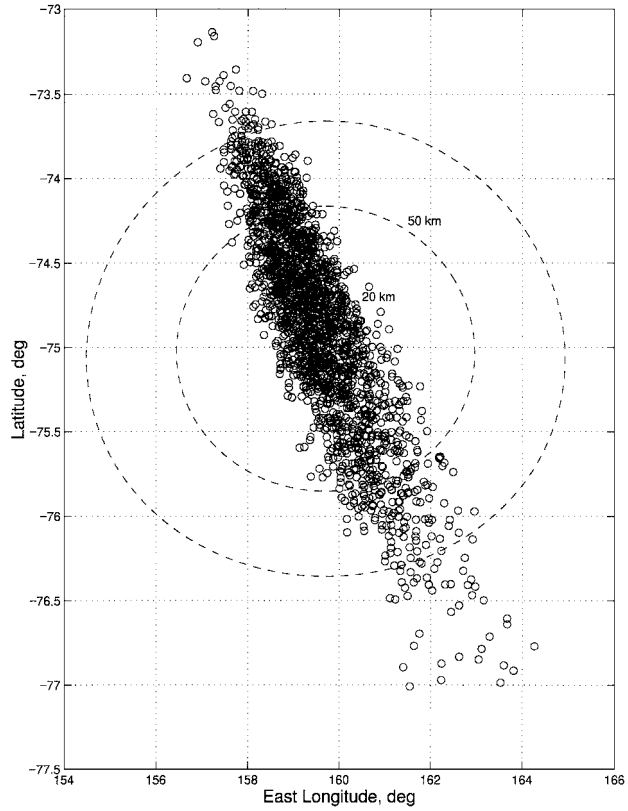

Fig. 21 Location of parachute deploy with 5-mm c.g. dispersions.

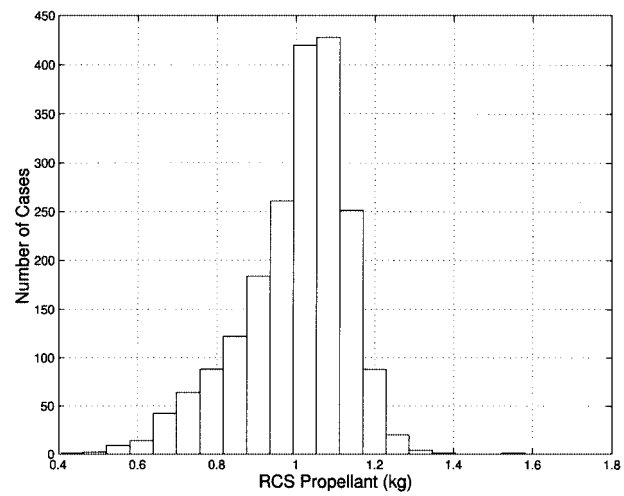

Fig. 22 Distribution of RCS usage with 5-mm c.g. dispersions.

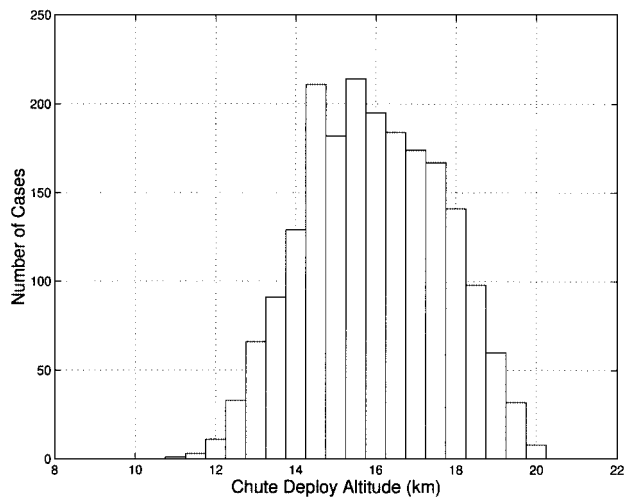

Fig. 23 Altitude of parachute deploy with 5-mm c.g. dispersions.

Conclusions

Subsequent to receipt of this analysis, the Mars Polar Lander project began using the modifications to the aerodynamic database discussed. An important verification of the entry heating was provided. Modifications were made to the entry autopilot in an attempt to reduce the size of the parachute-deploy footprint.

Based on LAURA CFD results, the use of the Mars Pathfinder aerodynamic database for Mars Polar Lander is appropriate. A scaling of the axial force coefficient serves to fine tune the database to compensate for variations due to geometry and trajectory differences. LAURA heating results show good agreement with LMA calculations. The recirculation region behind the vehicle extends less than two body lengths for the expected parachute-deploy conditions.

The mean parachute-deploy point is approximately 20 km short of the stated target, 75°S 160°E. Part of this discrepancy is because the vehicle is lighter than early predictions indicated. The parachute deploys approximately 1 km higher, though there is more spread than LMA estimated. As a result, the lower limit of parachute deploy is approximately the same. Again, the higher parachute-deploy altitudes result from a lighter vehicle. The LMA results showed Mach number at parachute deploy to be an amorphous function of parachute-deploy altitude, whereas the LaRC simulation showed chute deploy in a sharply defined Mach band. Doubling the lateral c.g. offset dispersions (to 5 mm) has a small impact on the overall performance.

References

[1] Braun, R. D., Powell, R. W., Engelund, W. C., Gnoffo, P. A., Weilmuenster, K. J., and Mitcheltree, R. A., "Mars Pathfinder Six-Degree-of-Freedom Entry Analysis," *Journal of Spacecraft and Rockets*, Vol. 32, No. 6, 1995, pp. 993–1000.

[2] Gnoffo, P. A., Gupta, R. N., and Shinn, J. L., "Conservation Equations and Physical Models for Hypersonic Air Flows in Thermal and Chemical Nonequilibrium," NASA TP-2867, Feb. 1989.

[3] Cheatwood, F. M., and Gnoffo, P. A., "User's Manual for the Langley Aerothermodynamic Upwind Relaxation Algorithm (LAURA)," NASA TM-4674, April 1996.

[4] Riley, C. J., and Cheatwood, F. M., "Distributed-Memory Computing with the Langley Aerothermodynamic Upwind Relaxation Algorithm (LAURA)," *Advances in Engineering Software*, Vol. 29, No. 3–6, 1998, pp. 317–324.

[5] Sutton, K., and Graves, R., "General Stagnation Point Convective Heating Equation for Arbitrary Mixtures," NASA TR-R376, Nov. 1971.

[6] Braur, G. L., Cornick, D. E., and Stevenson, R., "Capabilities and Applications of the Program to Optimize Simulated Trajectories (POST)," NASA CR-2770, Feb. 1987.

[7] Justus, C. G., "Mars Global Reference Atmospheric Model for Mission Planning and Analysis," *Journal of Spacecraft and Rockets*, Vol. 28, No. 2, 1991, pp. 216–221.

[8] Carpenter, J. R., "Delivery of Inertial Measurement Unit Model to Mars Surveyor '01 Atmospheric Flight Team," NASA Johnson Space Center Memorandum EG-97-103, Sept. 1997.

[9] Gnoffo, P. A., Weilmuenster, K. J., Braun, R. D., and Cruz, C. I., "Effects of Sonic Line Transition on Aerothermodynamics of the Mars Pathfinder Probe," AIAA Paper 95-1825, June 1995.

[10] "Mars Surveyor '98 EDL/MOI Verification Review," Lockheed Martin Astronautics, Denver, CO, April 1998.

R. D. Braun
Guest Editor